EKSPLOATACJA I NIEZAWODNOŚĆ MAINTENANCE AND RELIABILITY

Eksploatacja i Niezawodnosc – Maintenance and Reliability

Volume 23 (2021), Issue 1

journal homepage: http://www.ein.org.pl

Article citation info:
Ambrożkiewicz B, Syta A, Meier N, Litak G, Georgiadis A. Radial internal clearance analysis in ball bearings. Eksploatacja i Niezawodnosc – Maintenance and Reliability 2021; 23 (1): 42–54, http://dx.doi.org/10.17531/ein.2021.1.5.

Indexed by: Web of Science Group

Radial internal clearance analysis in ball bearings

Bartłomiej Ambrożkiewicz [a,c*], Arkadiusz Syta [b], Nicolas Meier [c], Grzegorz Litak [a], Anthimos Georgiadis [c]

[a] Department of Automation, Lublin University of Technology, ul. Nadbystrzycka 36, 20-618 Lublin, Poland
[b] Institute of Technological Systems of Information, Lublin University of Technology, ul. Nadbystrzycka 36, 20-618 Lublin, Poland
[c] Institute of Product and Process Innovation (PPI), Leuphana University, Universitätsallee 1, 21335 Lüneburg, Germany

Highlights

- Radial internal clearance in ball bearings is studied.
- Spectral and recurrence-based methods are applied for the time-series analysis.
- The optimal operating conditions of ball bearing are found.

Abstract

Radial internal clearance (RIC) is one of the most important parameters influencing on rolling bearing exploitation in mechanical systems. Lifetime of rotary machines strongly depends on a condition of applied rolling elements, thus a study on applied clearance is very important in terms of maintenance and reliability. This paper proposes, a novel approach of studying RIC, based on a nonlinear dynamics method called recurrences. The results are confronted with standard analyses, i.e. statistical condition indicators, Fast Fourier Transform and Continuous Wavelet Transform. The application of the mentioned methods allowed us to find the optimal radial clearance for operating bearings. To ensure precise measurements of the clearance, an automated setup for RIC measurements is applied and next mounted in a plummer block and tested to finally measure vibration acceleration. The proposed methods are useful for a condition monitoring and lifetime prediction of bearings or bearing-based systems in which a proper value of radial clearance is crucial.

Keywords

ball bearings; radial internal clearance; statistical analysis; recurrences; fast fourier transform; continuous wavelet transform.

1. Introduction

The trend of health condition monitoring (HCM) is introduced in many areas of industrial processes to ensure constant and maintenance free operation of machines and mechanical systems. Among many and different types of bearings, ball bearings play an important role in various mechanical mechanisms as they provide seamless rotational movement and carry radial load in most cases. However, bearing failure modes have various origins such as obsolescence, accidents or surface degradation and regarding this last, mechanical wear can be connected with corrosion, abrasion, adhesion or fatigue. Bearing lifetime and durability strongly depend on whether a bearing is correctly adjusted to a specific application regarding mostly operating conditions and several other features such as lubrication, loads, power losses, operating velocities, bearing characteristic frequencies etc. are taken into account in its selection.

One of the most important parameters in ball bearings being crucial for operation and having a strong influence on its dynamic response is radial internal clearance (RIC), determined as the play between rings and rolling elements. The selection of RIC in the ball bearing regarding its application is very important for both tribology and dynamics, and its optimal value has a strong impact on noise, generated vibrations, thermal expansion and fatigue [37]. In several works, the analysis of internal clearance in ball bearings was performed mostly based on the mathematical models. Tiwari et al. [41] discussed the influence of RIC on the dynamic response of a horizontal rotor, Harsha [14] studied the dynamics of a balanced rotor by variable radial clearance in time instead. Moreover, the influence of internal clearance on bearing life and damping ratio was referred by Yakout et al. [49] and Chudzik et al. [7] combined the FEM (Finite Element Method) model with the Lundberg-Palmgren fatigue theory. Miskovic et al. [32] analysed by thermo-graphic inspection how an amount of contamination in grease can influence RIC. Those works show the importance of internal clearance on bearing dynamics and nonlinear mathematical models of rolling bearings always refer to this parameter [42, 52].

Recently, the influence of bearing clearance on bearing performance has been increasingly studied to satisfy the high market demand for a reliable product [6, 17], especially for maintenance free applications. The development of online condition monitoring systems

(*) Corresponding author.
E-mail addresses: B. Ambrożkiewicz - b.ambrozkiewicz@pollub.pl, A. Syta - a.syta@pollub.pl, N. Meier - nmeier@leuphana.de, G. Litak - g.litak@pollub.pl, A. Georgiadis - georgiadis@leuphana.de

supposed to take into account changes of radial clearance [44] as its undesirable change in time can lead to premature wear. Xu et al. [48] applied the vibration analysis for studying bearing response with different clearance pointing the need for using optimal indicators in the analysis of spectra. Liu et al. [27] signalizes the fact that the obtained frequency spectra have stochastic character and one of the factors influencing them is radial clearance. Studies on bearing clearance are very demanding, and currently there is no accurate methodology for its detection in time. Conclusions coming from the state of the art works show the need to apply more accurate methods to analyse bearing dynamic response with different radial clearances.

Measurement of radial clearance in ball bearings is normalized and its principles are precisely described in the norm ISO-1132-2 regarding "Measuring and gauging principles and methods". In our research, an automated setup [30, 31] measures RIC in a self-aligning ball bearing, and the experiment is run with a precisely and accurately determined clearance in a bearing, analysing its dynamic response. For the analysis of experimental acceleration time series, recurrence analysis is proposed and evaluated both in qualitative (recurrence plots) and quantitative (recurrence quantificators) ways. Moreover, standard methods are used to confirm the dynamic states present in a bearing. For this case, statistical condition indicators and results of the Fast Fourier Transform (FFT) and Continuous Wavelet Transform (CWT) are discussed.

The recurrence method is effective at diagnostics in physiology, of manufacturing processes and faults in rotary systems. Focusing on the mechanical systems, Litak et al. [23, 25, 26] proposed in his works the application of recurrences to analyse nonlinear time series obtained from cutting and milling manufacturing processes. Kwuimy et al. [20-22] used the recurrence analysis to diagnose different systems by analysing results of mathematical models and experimental data. Fault diagnostics of rotary systems is discussed in other several papers [2, 24, 39]. The aim of our research is to analyse the dynamic response of a self-aligning ball bearing with different values of radial internal clearance.

According to the literature, radial clearance has a strong influence on bearing response, which is reflected in mathematical models. Currently, measurements of clearance are only performed on special test rigs or with instruments. There is no accurate method of its identification in-situ, except from using a gauge feeler on an assembled and non-rotating bearing. For this purpose, the recurrence analysis is applied in order to evaluate bearing dynamic response related to internal clearance. The results obtained from recurrences are compared with calculations of statistical indicators and frequency and time-domain digital signal processing (DSP) methods.

The remainder of this paper is structured as follows. The second section describes the experimental setup consisting of the automated system for measuring radial clearance and the test rig. Certain essential principles of the clearance measurement and experimental features are also specified here. The third section presents fundamentals of all applied diagnostics methods, focusing on the analysis of nonlinear time series and significance of the applied recurrence-based methods in the analysis of the systems. In the fourth section, the data is processed and the experimental results are discussed. The last section summarizes the paper and presents the next steps in the research.

2. Experimental setup and experiment description

The experimental setup consists of two test rigs: 1) an automated setup to measure radial clearance in ball bearings and 2) a gearbox equipped with plummer blocks dedicated to self-aligning ball bearings and a high precision inverter system to precisely set system's velocity. Both setups are in the laboratory of the Institute of Product and Process Innovation (PPI) at the Leuphana University of Lüneburg.

2.1. The automated setup for measuring bearing clearance

The first system presents a novel, very precise and fully automatized way of RIC measurements. The test rig is adapted to a wide range of ball bearings varying in external dimensions and type. For the experiment, a (SABB) 2309SK tapered bore double row self-aligning ball bearing is used in which bearing clearance can be roughly set with a clamping sleeve and nut. The digital measurement of RIC is performed according to the standardised method and its flowchart is presented in Figure 1. The concept of the setup can be introduced into industrial practice as it meets the requirements for Measurement System Analysis (MSA) by providing reproducible and repeatable clearance measurements. The software applied in the test rig is written in C language and its execution is managed with the Arduino Due

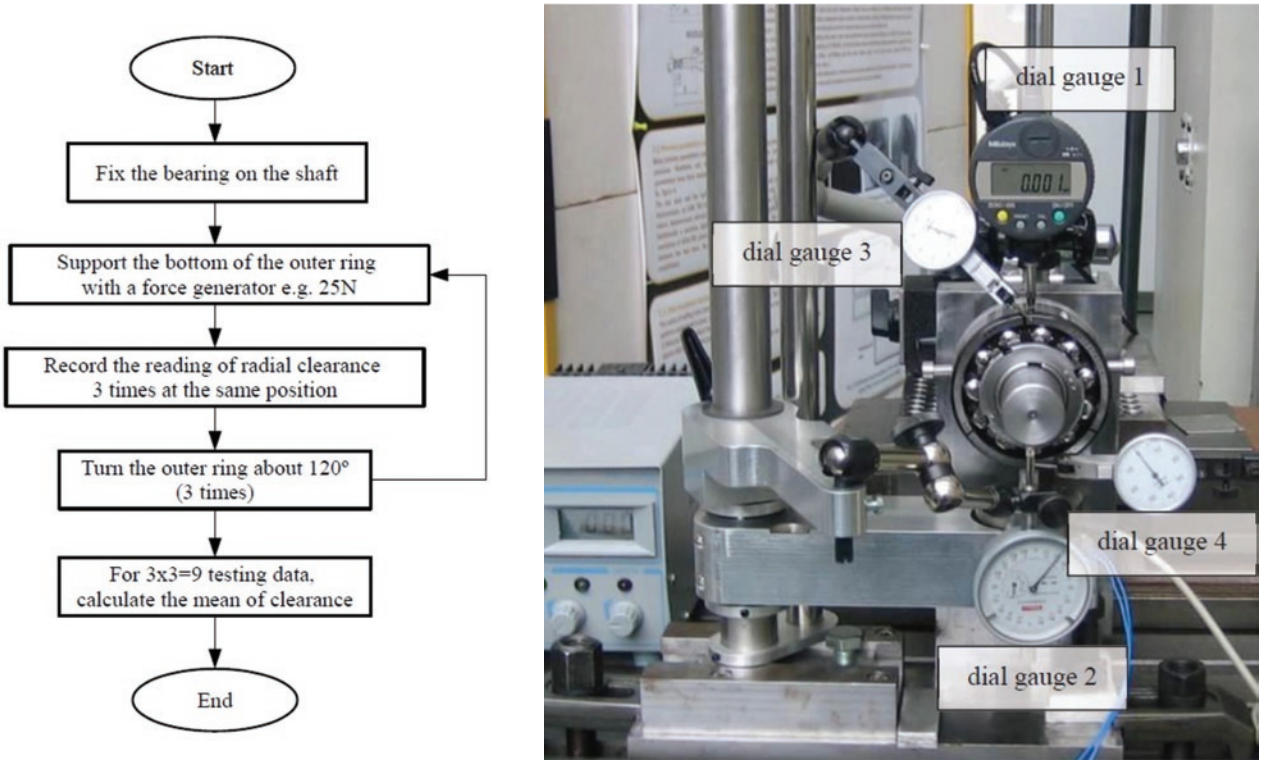

Fig. 1. Flowchart of RIC measurement procedure (left hand side), the automated setup for measuring bearing clearance (right hand side)

microcontroller. Four dial gauges in the setup are used to measure clearance, the distance of shifting the bearing onto the adapter sleeve and the influence of the test force on the displacement on the shaft.

2.2. Experimental gearbox

The bearing after the measurements is mounted into the plummer block (Figure 2) equipped with two accelerometers measuring bearing acceleration in two axes. The data is recorded with the piezoelectric (y-axis) and MEMS-based (x-axis) sensor with sampling time equal to 10.24ms, which corresponds to approximately 98Hz sampling frequency. The acceleration results are recorded with the data acquisition card (DAQ) in the CSV format and used in the further DSP analysis. Rotational velocity up to 50Hz (3000rpm) can be set on the test rig, but for the needs of the experiment, only one rotational velocity of 25Hz (1500rpm) is applied. The measurement for a single clearance lasts for around 10 minutes and is based on the obtained time series of acceleration, and the further DSP analysis is performed. The time of the experiment is fairly short so it is motivated to neglect a thermal expansion of the bearings during operation and ignore its influence on the clearance in contrary to the specially prepared cases [16, 33]. The influence of variable load is neglected as the measurements are focused on the impact of clearance on response. There are only constant loads generated by a housing and torque as a reaction from the rotating shaft. For the experiment, only brand-new bearings are used and it is assumed that there is no influence of characteristic bearing defects on the measured acceleration. In total, 6 cases with different clearances are studied. The detailed information on the applied testing setup and performed experiment are collected in Table 1 and 2, respectively.

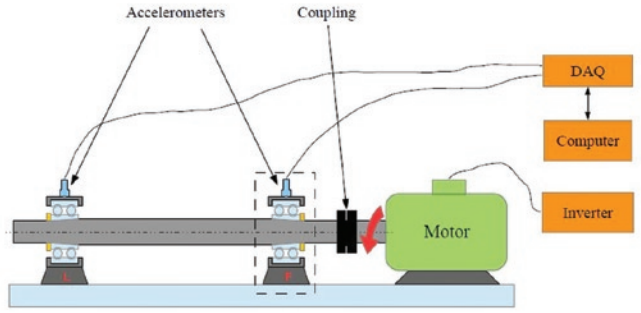

Fig. 2. Gearbox used for the bearing testing, the data were recorded in two axes only for the fixed bearing (right hand side)

Table 1. Equipment for the experimental setup.

Component	Type
Ball Bearing	NTN 2309SK
Adapter Sleeve	NTN H2309
Locating Ring	NTN FR 100x4
Bearing Housings	NTN SNC 511-609
MEMS Sensor	IFM VSA001
Piezoelectric Sensor	IFM VSP001
Data Acquisition System	IFM VSE100
3-Phase Motor	Siemens 1LA5090-4AA60-Z
Frequency Converter	Siemens SIMOVERT 6SE2103

Table 2. Duty cycle applied in the experiment.

Rotational velocity [rpm]	25Hz					
RIC [μm]	7	20	22	34	41	46

2.3. Ball bearing characteristic frequencies

The classical method used in diagnostics of ball bearing damages is based on the determination of characteristic frequencies related to the specific part [9, 35]. Each characteristic frequency has its own abbreviation in the industrial nomenclature. Their values depend on bearing's internal dimensions, features and rotational velocity. The basic characteristic frequencies for the NTN 2309SK bearing (Figure 3) are specified in Table 3 and the geometrical data are collected in Table 4.

Table 3. Ball bearing characteristic frequencies.

Characteristic frequency	Formula	Values of characteristic frequencies for SABB NTN 2309SK [Hz]
Fundamental Train Frequency (FTF)	$FTF = \frac{s}{2}\left(1-\frac{b_d}{d_p}cos\beta\right)$	0.394
Ball Spin Frequency (BSF)	$BSF = \frac{d_p}{b_d}s(1-\left(\frac{b_d}{d_p}cos\beta\right)^2$	2.160
Ball Pass Frequency (Inner Ring – BSFI)	$BSFI = \frac{n_b}{2}s\left(1+\frac{b_d}{d_p}cos\beta\right)$	7.884
Ball Pass Frequency (Outer Ring - BSFO)	$BSFO = \frac{n_b}{2}s\left(1-\frac{b_d}{d_p}cos\beta\right)$	5.116

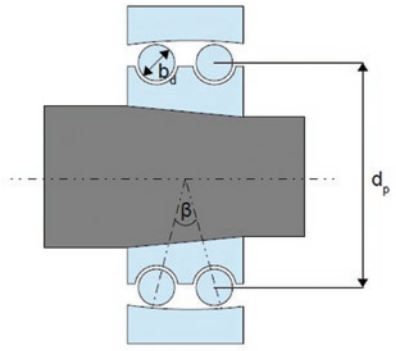

Fig. 3. Double row self-aligning ball bearing with its relevant dimensions marked taken for the calculation of its characteristic frequencies

The FFT and Wavelet results give the information about characteristic frequencies in the spectra and value of their amplitudes, and especially, the amplitude's value is taken into account to determine bearing damage. In this analysis, it is expected not to obtain high values of frequency peaks as the brand-new bearing is tested. The variable parameter is radial clearance and its different value influences the obtained frequency spectra.

Table 4. Ball bearing characteristic frequencies.

Parameters for the NTN 2309SK bearing	
Ball diameter b_d [mm]	15.870
Pitch diameter d_p [mm]	71.810
Contact angle β [°]	15.52
Number of rolling elements n_b [-]	26 (13 per row)
Rotational velocity s [Hz]	25

3. Diagnostics methods

Over the years, mostly frequency-domain DSP (Digital Signal Processing) methods such as FFT (Fast Fourier Transform), EMD (Empirical Mode Decomposition), SK (Spectral Kurtosis), etc. were applied in diagnostics of rotational systems. The relevant support for the frequency-based methods is the analysis performed in time domain as it allows us to observe and detect dynamic changes present in the system for a specific period of time. In this section, the principles of the applied methods to process experimental data are presented. Acceleration time-series are analysed with statistical condition indicators, the Fast Fourier Transform, the Continuous Wavelet Transform and Recurrences.

3.1. Diagnostics indicators applied to bearings diagnostics

The application of statistical condition indicators (CI) to the obtained time series from the experiment shows its accuracy in diagnostics of different kind of damages or transient states occurring in gears, bearings, shafts etc. [11, 28]. The mentioned indicators may be divided into time, frequency and time-frequency domain. In our experiment, we use only some of them, supposing their most significant impact on an identification of bearing response with different RICs.

1) Standard deviation (x_{std}) measures the dispersion of results regarding its mean and is calculated as the square root of variance [45]. The value of standard deviation corresponds to the amplitude of misalignment in the planar section:

$$x_{std} = \sqrt{\frac{1}{n-1}\sum_{i=1}^{n}\left(x_i - \bar{x}\right)^2} \tag{1}$$

2) Kurtosis (x_{kur}) defines how heavily the tails of a given distribution differ from the tails of a normal distribution. This indicator is applied to detect fracture [38] and wear [3] of components:

$$x_{kur} = \frac{\sum_{i=1}^{n}\left(x_i - \bar{x}\right)^4}{(n-1)x_{std}^4} \tag{2}$$

3) Crest factor (CF) is the ratio of instantaneous peak amplitude of a signal, to its root mean square RMS value. The mentioned parameter can diagnose different sources of impulsive vibrations (snaps and jerks) in the system [10]:

$$CF = \frac{x_0 - x_{pk}}{RMS_x} \tag{3}$$

4) Energy ratio (ER) is the ratio between a residual signal and a deterministic periodic signal which is separated using an autoregressive model. With the ER, there is a high possibility to detect strong wear or defect [51]:

$$ER = \frac{RMS_d}{RMS_{y_d}} \tag{4}$$

3.2. Fast Fourier Transform (FFT)

The Fast Fourier Transform as the most popular DSP method used in diagnostics of mechanical structures provides the information on characteristic frequencies present in spectra [1]. The analysed time-series is decomposed into a number of sinusoidal signals characterised by specific frequency. Information of potential damage of the system is presented on a spectrogram which consists of characteristic frequency peaks with determined amplitude. In the case of strongly nonlinear and non-stationary data, the FFT loses the information about time, so there is no possibility to define how long a specific state lasts. Additionally, noise present in experimental time-series introduces additional frequency peaks which can mix with other relevant peaks denoting damage so a band-pass filter is necessary [8].

In the analysis of discrete signals $x[n]$, the discrete Fourier transform (DFT) can be described in the following way [34]:

$$X(k) = \sum_{n=0}^{N-1} x[n] e^{-j\left(\frac{2\pi nk}{N}\right)} \tag{5}$$

where: N is the harmonic index regarding the exponential function for k=0,1,…,N-1.

In the final analysis with the FFT, the scaling of the spectrum is necessary in frequency units, and each signal $X(k)$ is attributed to frequency $f[k]$ according to the following formula:

$$f[k] = k\frac{f_p}{N} \tag{6}$$

where: f_p is sampling frequency.

3.3. Continuous Wavelet Transform (CWT) and Scale Index (SI)

The disadvantage of the FFT is eliminated with an application of the Wavelet Analysis by complementing it with a localisation of periodicities in time. In the analysis of mechanical systems, it is important to detect transient and intermittent phenomena which can occur in short periods of time. The window size is crucial in time series analysis in time and frequency resolution. Owing to wavelets analysis, the window size is adapted to the identified state in the signal: it narrows when focusing on high-frequency or small-scale features and widens on low-frequency or large-scale features like in zoom lens with adjustable focus [15].

The mathematical definition of the continuous wavelet transform regarding acceleration time series has a following form:

$$W_{s,n}(Acc) = \sum_{i-1}^{N}\frac{1}{s}\left(\frac{i-n}{s}\right)\frac{\left(Acc(t_i) - \langle Acc\rangle\right)}{\sigma_{Acc}} \tag{7}$$

where $<Acc>$ and σ_{Acc} are average and standard deviations of acceleration, s denotes the scale index and n is the time index.

The wavelet power spectra (WPS) of the signal is defined as the squared modulus of the CWT and is the following:

$$P_w = \left|W_{s,n}\right|^2 \tag{8}$$

Another wavelet-based tool is the Scale Index (SI) proposed by Benitez et al. [4, 5]. Notably intended for non-stationary time-series, this index provides the quantitative measure of signal's non-periodicity. A scalogram of a given analysed signal has the following form:

$$S(s) = \left(\int_{c(s)}^{d(s)} \left|WAcc(u,s)\right|^2 du / (d(s) - c(s)) \right)^{\frac{1}{2}} \tag{9}$$

where *WAcc(u,s)* is the CWT of the signal at specified time u and scale s.

The scale index interval $[s_0,s_1]$ is determined as the quotient:

$$i_{scale} = \frac{S(s_{min})}{S(s_{max})} \tag{10}$$

where s_{max} is the maximum in the scale index interval and s_{min} is the minimum defined in the left scale interval after the maximum and s_1. The result of the scale index is from zero to one, which quantifies the measure of non-periodicity of the signal. The value close to one denotes the strongly nonlinear signal and value close to zero denotes the periodic signal.

3.4. Recurrence-based methods

In the analysis of strongly nonlinear experimental time series, the statistical and DSP analyses should be supported with an alternative method showing changes in short-time intervals. One of the possible methods is recurrence analysis. Experimental data are mostly characterized by strong nonlinearities and noise, so recurrences are a promising method in our analysis. A change in the RIC value can cause changes in the dynamic response of the analysed system that can be identified by recursion analysis. Recurrence is understood here as the property of the dynamical oscillator when a specific state of the system returns to the previous one after some time. Firstly, the idea of recurrences was proposed by Henri Poincare in his seminal work to analyse conservative systems. In order to visualise trajectories of dynamic systems, Eckmann et al. [12] introduced the recurrence plots (RP) method designed to locate hidden recurring patterns, non-stationarity and structural changes. In further research, this method was extended by Webber et al. [46, 47] and Marwan et al. [29] by statistics of points as well as diagonal and vertical lines from recurrence plots.

The next step in the development of recurrence-based methods was the introduction of the recurrence quantification analysis (RQA) [50] in which recurrence quantificators show quantitative information from recurrence plots. Nowadays, in many research, both recurrence plots and recurrence quantification analysis approaches are applied to both experimental and modelled nonlinear systems from many fields.

3.4.1. Recurrence plots method

The principle of the RP-based method is revealing all times when the phase space trajectory of the dynamical system meets roughly the same area in the phase space. Two points on the trajectory are considered as neighbours when they are close enough to each other and this can be expressed with the R distance matrix with its element R_{ij}^{ε} calculated as follows:

$$R_{i,j}^{\varepsilon} = H\left(\varepsilon - \left\|\mathbf{x}_i - \mathbf{x}_j\right\|\right), i,j = 1,\ldots,N \tag{11}$$

where N is the number of considered states $\mathbf{x}_i$, $\mathbf{x}_j$ for a threshold distance ε, $\|\ \|$ a norm and H the Heaviside function. The obtained matrix consisting of zeros and ones denotes corresponding recurrence plots by:

$$R_{i,j} = \left\{ \frac{1 : \{\mathbf{x}_i\} \approx \{\mathbf{x}_j\}}{0 : \{\mathbf{x}_i\} \neq \{\mathbf{x}_j\}} \right\}, i,j,...,N \tag{12}$$

where $\{\mathbf{x}_i\} \approx \{\mathbf{x}_j\}$ indicates points coordinates in the embedding dimension space belonging to the neighbourhood of radius ε. To obtain the recurrence plot, we need three following parameters, i.e. threshold - ε, embedding dimension - m and time delay – τ to create missing coordinates [40]. The threshold value is a maximal distance that marks two points as a recurrence. There are several approaches including percentage of standard deviation of data, but usually a few percent of recurrence points is sufficient. The time delay should be optimal to preserve both short and long term correlations (autocorrelation method or mutual information method [13]). The value of embedding dimension must ensure the situation when there are no false neighbours in the reconstructed attractor (false neighbours method [18]). On the other hand, instead of reconstructing the attractor, it is possible to apply the recorded data in the plummer block. In our case, these are acceleration time series measured in two directions: x and y as components of the state vector that clearly describe the dynamics of the system at a given time. This approach avoids errors due to improper reconstruction and was adopted in this work.

3.4.2. Recurrence quantification analysis

The recurrence quantification analysis (RQA) provides a quantitative interpretation of obtained recurrence plots quantifying the number and the duration of recurrences for the analysed dynamic system within its state space trajectory. The three main recurrence quanitifactors are the recurrence rate (RR) based on a recurrence points density, determinism (DET) based on diagonal lines statistics and laminarity (LAM) based on vertical lines. The appearance of a diagonal line on the recursive chart indicates periodicity and the length of this line. The appearance of a vertical line on the recursive graph indicates a laminar state when the system is stuck for a time equal to the length of the line in one specific state. Both statistics can be used to detect the system switching between its various states.

(1) Recurrence Rate (RR) describes the density of recurrence points on the recurrence plot:

$$RR = \frac{1}{N^2} \sum_{i,j=1}^{N} R_{i,j} \text{ for } |i-j| \geq 1 \tag{13}$$

(2) Determinism (DET) expresses the percentage of recurrence points creating diagonal lines in the recurrence plot of minimal length l_{min}:

$$DET = \frac{\sum_{l=l_{min}}^{N} lP(l)}{\sum_{l=l_{min}}^{N} P(l)} \tag{14}$$

(3) Laminarity (LAM) represents the ratio between recurrence points forming vertical structures:

$$LAM = \frac{\sum_{v=v_{min}}^{N} vP(v)}{\sum_{v=v_{min}}^{N} vP(v)} \tag{15}$$

(4) Diagonal line (L) $R_{i+k,j+k} \equiv 1 \Big|_{k=0}^{l-1}$ occurs when a segment of the trajectory runs almost in parallel to another segment for l time units:

$$\mathbf{x}_i \approx \mathbf{x}_j, \mathbf{x}_{i+1} \approx \mathbf{x}_{j+1}, \ldots, \mathbf{x}_{i+l-1} \approx \mathbf{x}_{j+l-1} \tag{16}$$

A diagonal line of length l is then defined by:

$$\left(1 - R_{i-1,j-1}\right)\left(1 - R_{i+l,j+l}\right)\prod_{k=0}^{l-1} R_{i+k,j+k} \equiv 1 \tag{17}$$

The length of this diagonal is determined by the duration of such similar local evolution of trajectory segments.

(5) Vertical line (V) $R_{i,j+k} \equiv 1 \Big|_{k=0}^{v-1}$ marks a time interval in which a state does no change or changes very slowly:

$$\mathbf{x}_i \approx \mathbf{x}_j, \mathbf{x}_{i+1} \approx \mathbf{x}_{j+1}, \ldots, \mathbf{x}_{i+v-1} \approx \mathbf{x}_{j+v-1} \tag{18}$$

The formal definition of a vertical line is:

$$\left(1 - R_{i,j-1}\right)\left(1 - R_{i,j+v}\right)\prod_{k=0}^{v-1} R_{i,j+k} \equiv 1 \tag{19}$$

4. Data analysis and results

In this section, we report the results of all applied methods for the acceleration results obtained from the experiment for bearing response differing from each other in radial clearance values. In order to distinguish the differences between experimental cases, firstly, the statistical indicators were calculated for time series consisting of 15000 data points, the results from each sensor were analysed separately, rotational velocity during the test was chosen n=1500 rpm.

Table 5 (x-axis) and Table 6 (y-axis) show the results of the most statistical indicators. The results obtained differ in values in a certain order. The standard deviation results for both axes have a decreasing tendency till RIC=22μm, whereas its value has an increasing trend in the next cases. The low value of STD can be related to low amplitudes obtained in the signal, and consequently, there are low amplitudes of horizontal and vertical accelerations in the bearing.

The results of kurtosis are different in nature in each axis. For the x-axis in the area of interest, RIC=22μm kurtosis has the maximum value. In contrast, for the y-axis for the same value of RIC, the kurtosis has the minimum. However, the trend of that value is kept and the values of kurtosis in all cases are close to 3, which indicates a Gaussian-like peakedness. The leptokurtic (more peaky distribution, Kurt>3) and platykurtic (flatter than Gaussian distribution, Kurt<3) shapes of distribution in different axes are caused by the subjected load and the torque acting on the bearing from the shaft, which influences differently on each accelerometer. For the larger kurtosis of time series, the dynamical system is close to pass intermittency between two solutions [36].

The distribution of the crest factor (CF) values is similar to the previous indicator: single transient peaks in the time course cause an increase of the CF in relation to the small standard deviation value of the signal. The correlation between the RIC value and the mentioned indicator is observed in the energy ratio values of the signal, for both axes. This means that the residual signal is richer for the smaller values of clearance, which is related to a tight deployment of rolling surfaces resulting in increased friction or amplitude of contact stresses.

Based on statistical indicators results, we conclude that there is a correlation between increasing RIC values and corresponding indicators. Note, standard deviation and kurtosis show non-monotonic

Table 5. Values of statistical indicators for the results obtained from the x-axis at 25Hz.

RIC [μm]	Standard deviation σ [m/s^2]	Kurtosis	Crest Factor	Energy Ratio
7	18.448	3.097	1.148	0.441
20	18.201	3.126	1.132	0.391
22	9.629	3.356	1.190	0.362
34	22.003	3.071	1.140	0.378
41	32.593	2.926	1.150	0.335
46	33.839	2.972	1.177	0.337

Table 6. Values of statistical indicators for the results obtained from the y-axis at 25Hz.

RIC [μm]	Standard deviation σ [m/s^2]	Kurtosis	Crest Factor	Energy Ratio
7	3.678	2.974	1.117	0.409
20	3.547	3.081	1.127	0.370
22	1.847	2.641	1.145	0.349
34	3.606	3.476	1.120	0.326
41	5.064	2.771	1.111	0.322
46	4.848	3.202	1.128	0.313

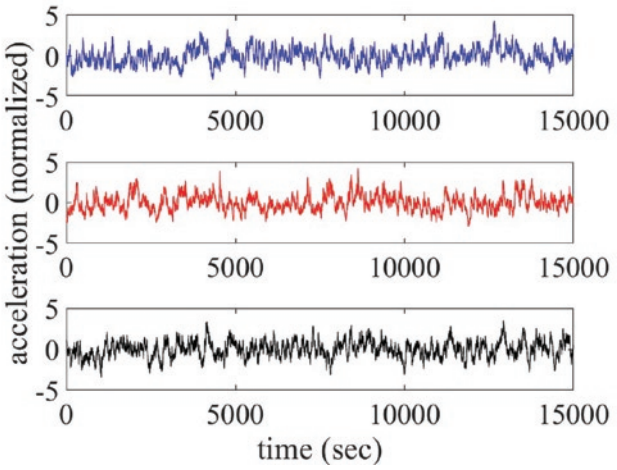

Fig. 4. Normalized acceleration time series obtained from the x-axis for the selected clearance of RIC=20μm – blue, 22μm – red and 34μm – black

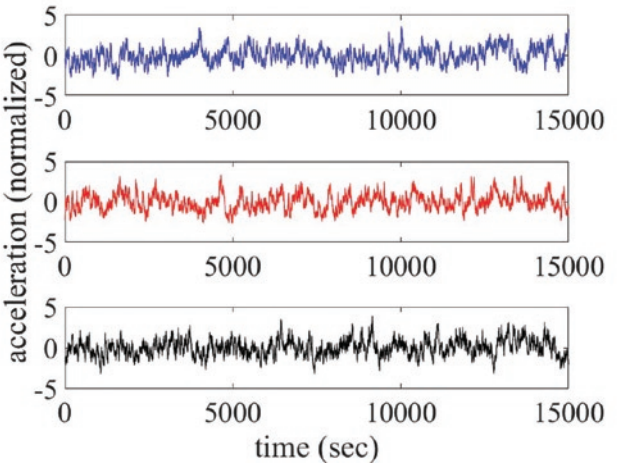

Fig. 5. Normalized acceleration time series obtained from the y-axis for the selected clearance of RIC=20μm – blue, 22μm – red and 34μm – black

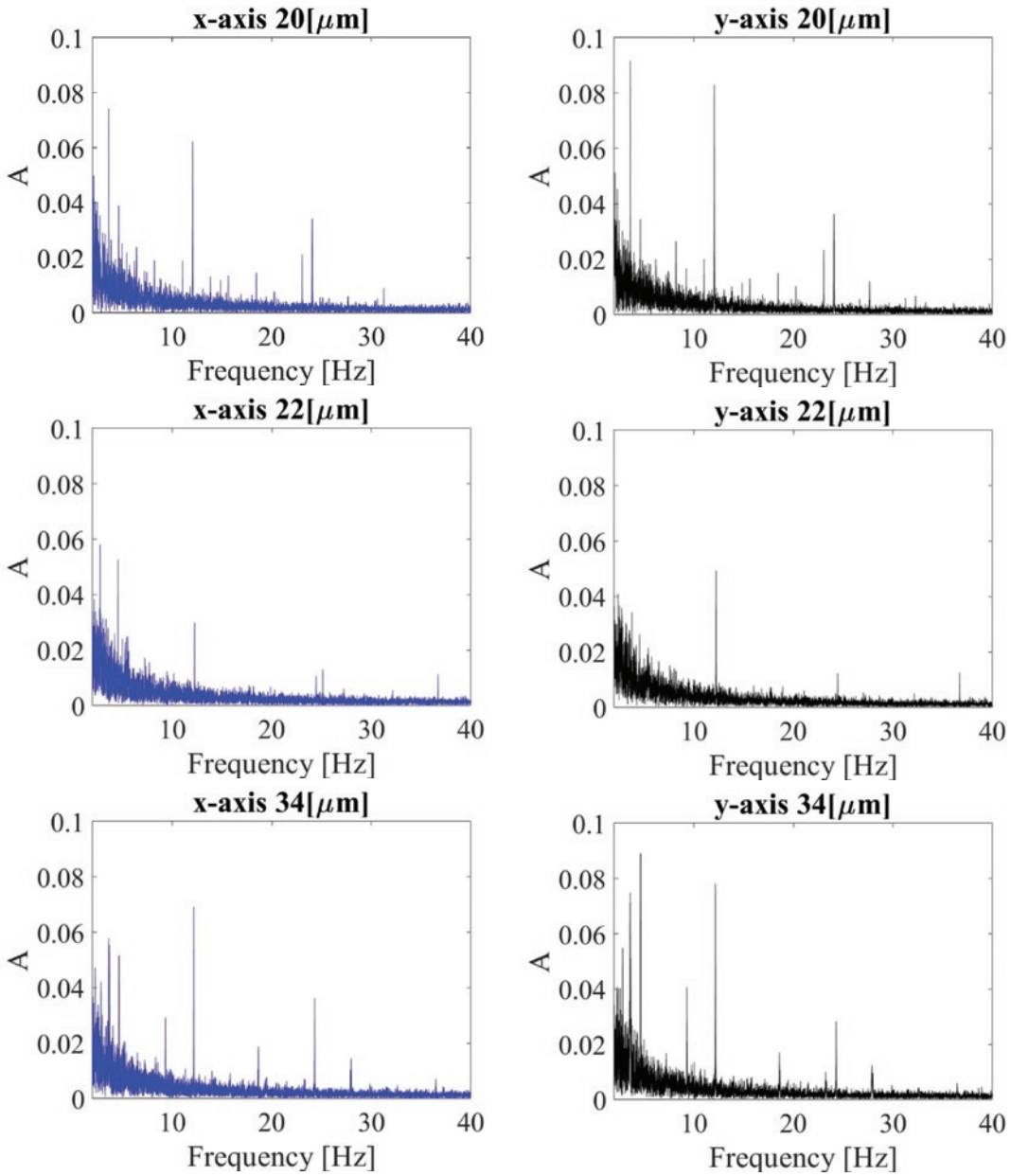

Fig. 6. Results of the FFT (Fast Fourier Transform) for the time series obtained from the x-axis (left panel) and the y-axis (right panel) for the selected clearance of RIC=20, 22 and 34μm (downwards)

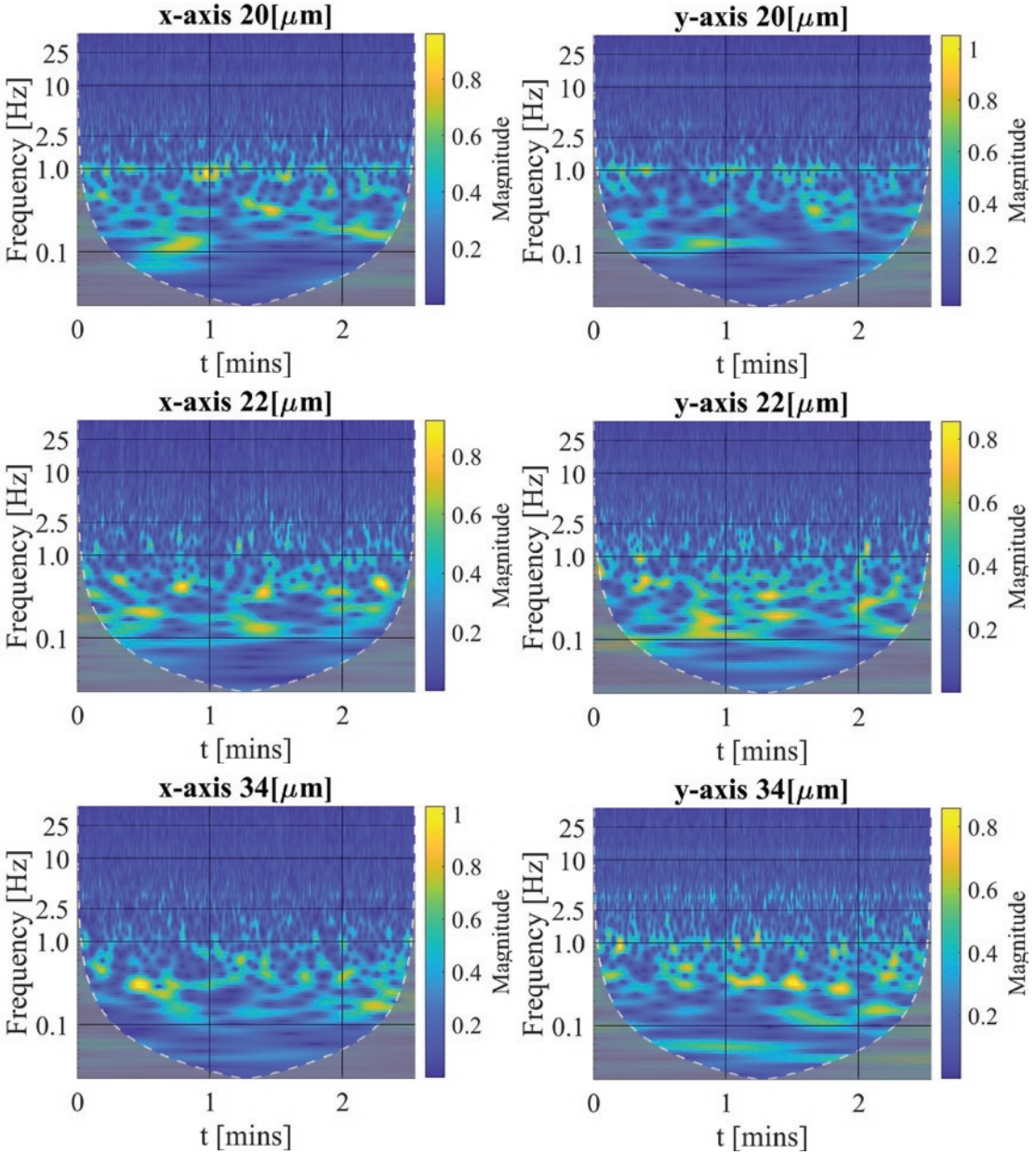

Fig. 7. Results of the CWT (Continuous Wavelet Transform) for the time series obtained from the x-axis (left panel) and the y-axis (right panel) for the selected clearances of RIC=20, 22 and 34μm (downwards)

dependence on RIC values, while the crest factor is almost constant and the energy ratio has a decreasing trend. The statistical indicators provide some information about dynamics of the bearing system, however it is difficult to draw more specific conclusions. One of the approaches is the calculation of the Fast Fourier Transform for the area of interest, cases RIC={20;22;34}[μm] for the corresponding acceleration time courses in the x and y axis (Figure 6). In all cases, the basic bearing's characteristic frequencies specified in Table 3 are observed, all of the peaks have small amplitude, so the bearing used in the experiment is not damaged. However, the frequency spectra for the specific clearance differ from each other by the number of additional peaks enriching the response. The spectra for RIC=22μm have less complex spectra with the least number of frequency peaks, and the only one main harmonic and few smaller frequency peaks are observed. For RIC=20μm instead the share of small peaks is relatively bigger than for RIC=34μm, which is connected with increased nonlinearity in the response.

As the relevant information about the time is lost by the FFT analysis, the Continuous Wavelet Transform is used. The resulting WPS for acceleration time series for RIC={20,22,34} are depicted in Figure 7. The yellow and blue areas on the scalograms represent the highest and lowest power levels, respectively, with the other colours referring to the intermediate power level. The grey area below the white dashed U-shaped line represents the cone of influence (COI), i.e. the region of wavelet spectrum in which edge effects become important and is defined as the *e*-folding time for the autocorrelation of wavelet power at each scale [43]. The rest of the scalogram should only be considered for further interpretation and represents the regions of greater than 95% confidence.

The characteristic frequencies found with the FFT are also depicted on the scalograms by the stronger and weaker yellow zones. The observed strong noise in the spectrogram by low frequencies is deposited on the scalograms. In all cases, the yellow areas are focused around the frequency of 0.4Hz, which relates to the Fundamental Train Frequency and is observed in the entire analysed signal with single gains in the power spectra. Besides, stronger but short periodic tendencies and intermittent behaviour can be observed in the frequency interval of [0.1, 1]Hz (Figure 7). Both sensor channels fixed on the x and y axes show similar results in terms of frequencies. The differences between clearance cases related to the amplitude of peaks are also visible, by 20 and 34μm, the area around the frequencies 12.5 and 25Hz is definitely stronger it is constant by entire time-course. For 22μm, the

power spectra are fairly diminished for the mentioned frequencies, but the dominate frequencies are shown in the numerous and very short time-intervals from the extended frequency range *f*=[0.1;10Hz]. This fact can be connected with the results obtained by calculated the condition indicators and FFT, assumedly by RIC=22μm as there is the most quiet (stable) bearing operation. The contact between balls and raceways is well fitted, resulting in low amplitude horizontal and vertical displacement.

In order to quantify the found observations in the CWT scalograms, Inner scalograms and Scale Index Analysis (SIA) are performed (Figure 8, Table 7). Note that for both sensors the inner scalograms are showing a small corrugation of the RIC=22 μm case (see the red lines in Figure 8) in contrast to the other cases. The SIA results obtained proved that the lack of higher amplitudes of vibration, improving bearings rotational character of motion can be found in the case of RIC=22μm (Table 7). The course in scale domain has the most smooth character and estimated SI is almost 1.0, relating to its high regularity in the rotational motion in frequencies from the range of *f*=[10;45]Hz. This interval was chosen to neglect the sampling noise oscillations.

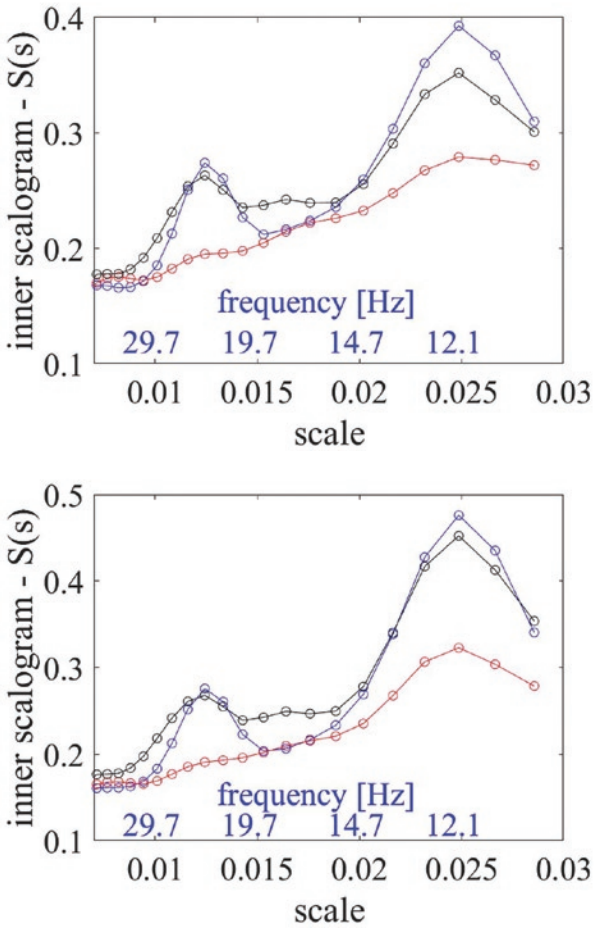

Fig. 8. Results of Scale Index Analysis (SIA) for the acceleration time courses obtained from the x-axis (top) and y-axis (bottom). Colours of the lines denote the following RIC values: blue - 20μm, red - 22μm, black - 34μm

Table 7. Values of Scale Index

RIC [μm]	x-axis	y-axis
20	0.77	0.73
22	about 1.00	about 1.00
34	0.89	0.89

The described observations and remarks are more or less visible on the recurrence plots (Figure 9); all of them represent different kinds of patterns which are differing from each other in distribution of the recurrence points. In order to visualise them, one of the short-time series consisting of 1500 data points was taken into account. The cases of RIC=20 and 34μm represent more periodical character. The obtained recurrence points are close to each other, which means non-chaotic and ordered response. In the other case, the concentration of recurrence points has no specific structure. By almost the same percentage of RR, they are dispersed, which proves intermittences in the bearing response. The characteristic diagonal and vertical line structures clear in all recurrence plots (Figure 9) are related to periodic motion with

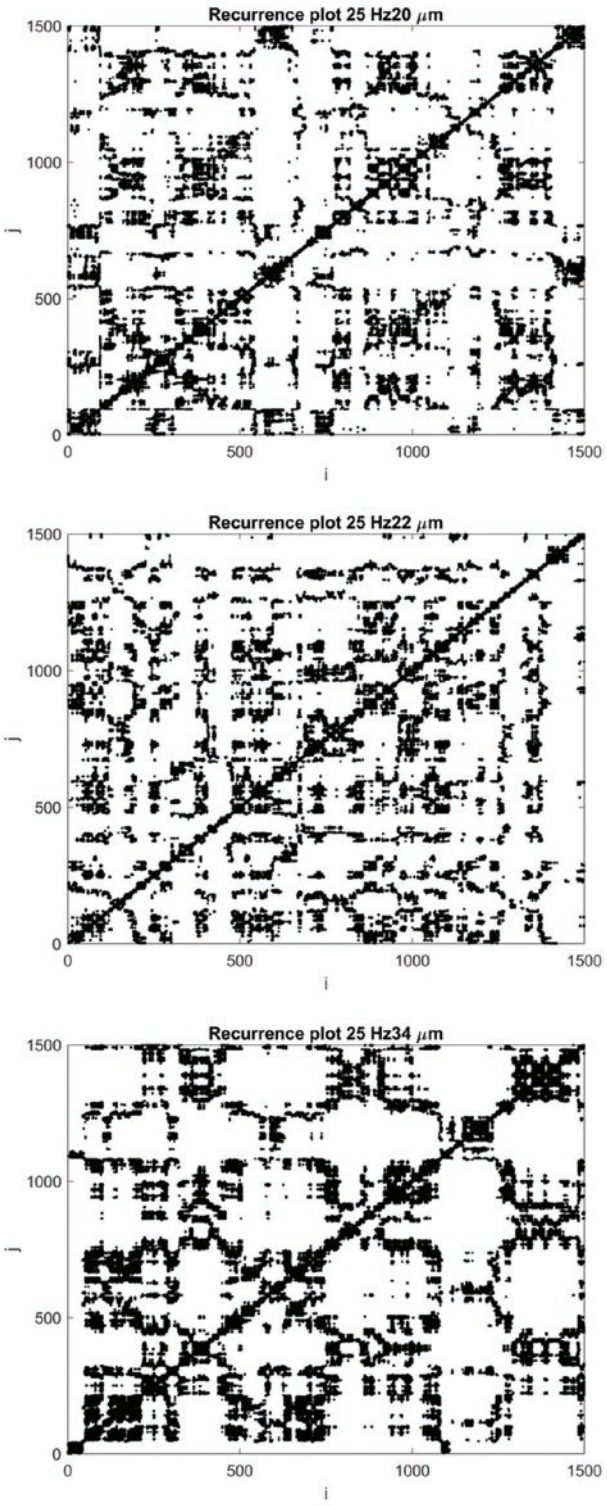

Fig. 9. Recurrence plots for RIC=20μm (top), RIC=22μm (middle) and RIC=34μm (bottom)

Table 8. Results of recurrence quantificators for the considered cases derived from random short time series

RIC [μm]	RR	DET	LAM	L_{MAX}	V_{MAX}
20	0.045	0.81	0.89	50	31
22	0.045	0.76	0.86	53	21
34	0.078	0.87	0.92	72	42

the periods defined by the vertical (or horizontal) space between lines and left in the current state, respectively. On the other hand, the square like structures signal occurrence of intermittences [19].

To quantify the nonlinearity of frequently appearing intermittencies in response and multiple solutions, recurrence quantification analysis is applied. In particular, the recurrence quantificators such as RR, DET, LAM, L_{MAX}, V_{MAX} were calculated. The method is mostly dedicated to analysing short time series so, at first, the long signal was divided into 10 parts consisting of 1500 data points each. Next, the value of a given quantificator was calculated in each short signal, then the final value taken for the evaluation was the average of the collection of results. For the calculation of each quantificator and plotting

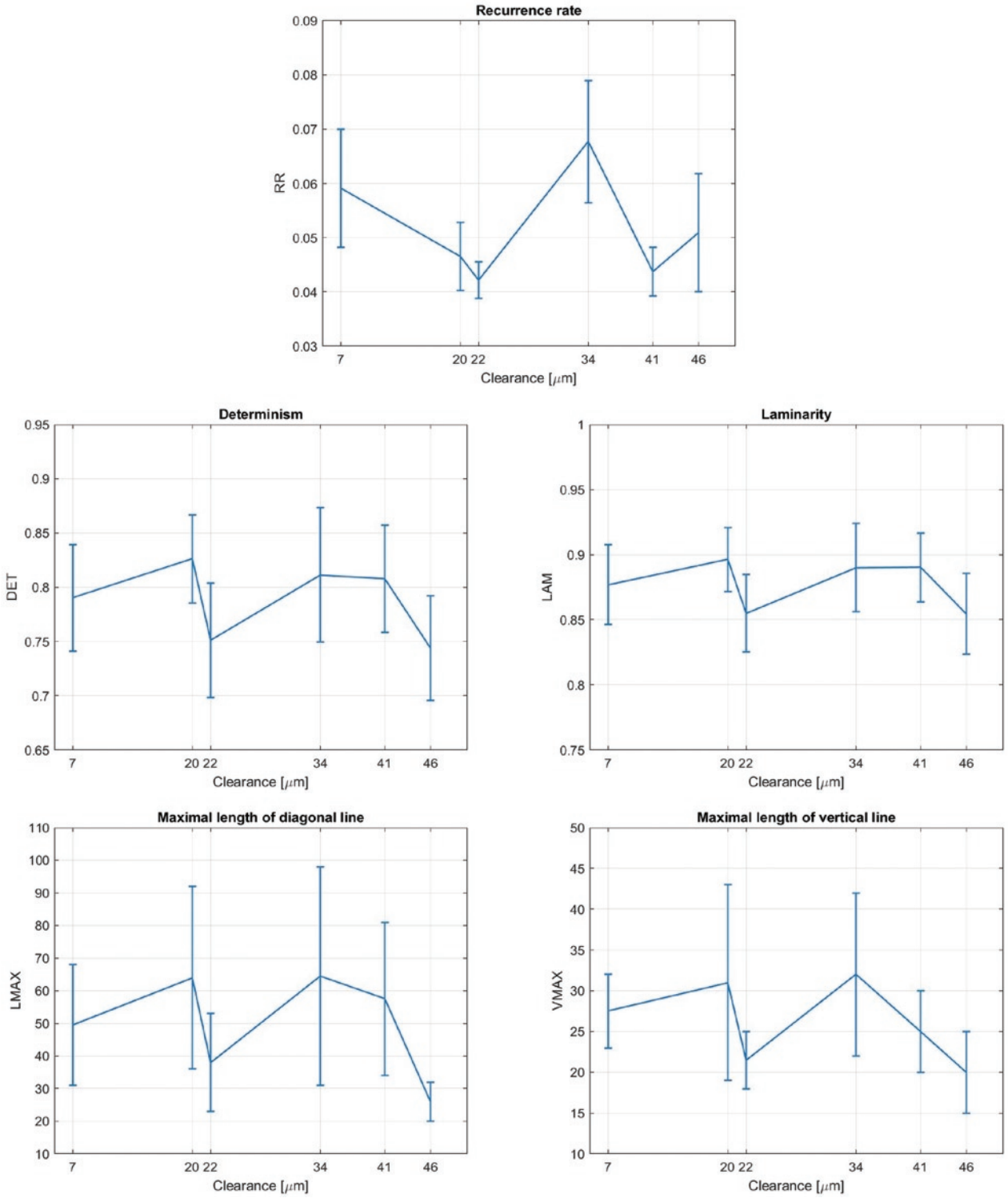

Fig. 10. Plots of the recurrence quantificators with a marked error range versus clearance

the recurrence plots, the constant threshold value was taken as ε=0.4. In Table 8, exemplary results of quantificators are collected for one random short time series. All of them are visualised on the plots with a marked error range formed out of the minimum and maximum value of each quantificator (Figure 10).

Regarding the obtained values of recurrence rate (RR), they correspond to the percentage of recurrence points obtained on the recurrence plots. The only correlation is the increase in the amount of the recurrence points with the increased RIC value by the same level of threshold.

Determinism (DET) corresponds to predictability of the system and again the averaged minimum is in RIC=22μm. The lower value of determinism, the system behaves more unpredictably, which proves the occurrence of the transient state in the bearing. The error value varies almost in the same range for all clearances.

The next considered quantificator is laminarity (LAM). Similarly to determinism, its averaged minimum value is in RIC=22μm. Laminarity corresponds to mean time when the state of the system is "trapped" for some state and indicates a switching between different states of the system.

The L_{MAX} increases with the RIC value. For the middle one, however, it can be observed that it changes in a relatively narrow range against the neighbouring. Variability of the length of diagonal lines does not clearly inform about a specific bearing clearance and does not precisely define the transient state for the clearance of 22μm.

In the case of V_{MAX}, the length of vertical lines refers to small variations in recurrences and isolated points mean large changes. Regarding vertical lines length, there is the same values distribution as for laminarity and determinism. Moreover, the values for RIC=22μm change in low and narrow ranges, showing its non-linear origin transition into optimal bearing operation conditions.

5. Discussion and conclusion

In this paper, the tests on a double row self-aligning ball bearing with different values of radial internal clearance. The analysis of its acceleration response was evaluated with the statistical indicators, the FFT, the CWT and the recurrence-based methods. It should be emphasized, that the research system was not damaged, but with a changed operational parameter having a strong influence on its dynamic behaviour. The initial analysis of the bearing response with the statistical indicators allowed us to find the transient point in the bearing characterized by one value of RIC. With the FFT and CWT, it was possible to find the characteristic frequencies present in the spectra and visualize them in time domain. The results of Scale Index proved the differences in the disturbance of the vibrations in the bearings operation between the acceleration signals obtained for the different values of radial clearance. The application of the selected recurrence quantificators and recurrence plots supported the analysis and showed the unstable behaviour of the bearing. In the performed, two specific limits of bearing behaviours can be distinguished. The first one is a frictional solution for fairly small RIC values where at small distance between rolling surfaces introduces friction. It can be connected with an undesirable skidding phenomenon in ball bearings. In the second limit, an uninhibited movement of rolling elements with contact loose and impacts is obtained. On the other hand, the point for RIC=22μm is the range between them, where the frequency response is changing in terms of kurtosis (Table 5 and 6) by indicating vicinity to intermittency and also in the recurrence plot (Figure 9), where the multi-scales in self-organization of the black area is stronger for RIC=22μm.

To sum up the four different methods allow for identifying and visualize transient states occurring in the ball bearing by different values of radial internal clearance. The state can be related to a negative phenomenon called skidding and such an unexpected behaviour was observed on the plots of all applied recurrence quantificators. The recurrence rate (Figure 10) shows that the repetitions of the states are strongly comparable to the case of RIC=22μm to the other neighbouring cases. Simultaneously, determinism and laminarity show a clear decrease to signal relative decrease of periodicity and the slower changes. Furthermore, the maximal diagonal and vertical lengths reductions express the unpredictability (chaoticity or stochasticity) of the optimal solution of RIC=22μm. Note that the other decreases of the quantificators may not correspond to the optimal choice of clearance for the other reasons as durability of bearings.

The applied methods have the potential and further steps in research will consider testing at different rotational velocities, for longer time series and on a greater number of tapered bore self-aligning ball bearings to set a specific bearing clearance in the same bearing. More complex tests would increase the power of the test and introduce the new methods (CWT, SIA and Recurrences) into diagnostics of the dynamic behaviour of bearings' dynamic behaviour. The performed tests showed more or less the range of optimal clearance can be neither small nor big to avoid spalling or pitting.

References

1. Al-Badour F, Sunar M, Cheded L. Vibration analysis of rotating machinery using time-frequency analysis and wavelet techniques. Mechanical Systems and Signal Processing 2011; 25(6): 2083-2101, https://doi.org/10.1016/j.ymssp.2011.01.017.
2. Ambrożkiewicz B, Meier N, Guo Y, Litak G, Georgiadis A. Recurrence-based diagnostics of rotary systems. IOP Conference Series: Materials Science and Engineering 2019; 710 012014, https://doi.org/10.1088/1757-899X/710/1/012014
3. Bechhoefer E, Qu Y, Zhu J, He, D. Signal processing techniques to improve and acoustic emissions sensor. Annual conference of the prognostics and health management 2013; 4: 1-8.
4. Benitez R, Bolos V J, Ramirez R. A wavelet-based tool for studying non-periodicity. Computers and Mathematics with Applications 2010; 60: 634-641, https://doi.org/10.1016/j.camwa.2010.05.010.
5. Bolos V J, Benitez R, Ferrer R. A new wavelet tool to quantify non-periodicity of non-stationary economic time series. Mathematics 2020; 8(5), https://doi.org/10.3390/math8050844.
6. Castilla-Gutierrez J, Fortes J C, Pulido-Calvo I. Analysis, evaluation and monitoring of the characteristic frequencies of pneumatic drive unit and its bearing through their corresponding frequency spectra and spectral density. Eksploatacja i Niezawodnosc - Maintenance and Reliability 2019; 21(4): 585-591, https://doi.org/10.17531/ein.2019.4.7.
7. Chudzik A, Warda B. Effect of radial internal clearance on the fatigue life of the radial cylindrical roller bearing. Eksploatacja i Niezawodnosc - Maintenance and Reliability 2019; 21(2): 211-219, https://doi.org/10.17531/ein.2019.2.4.
8. Climente-Alcaron V, Antonino-Daviu J A, Haavisto A, Arkkio A. Particle filter-based estimation of instantaneous for the diagnosis of electrical asymmetries in induction machines. IEEE Transactions on Instrumentation and Measurement 2014, 63(10): 2454-2463, https://doi.org/10.1109/TIM.2014.2310113.
9. D'Elia G, Cocconcelli M, Mucchi E. An algorithm for the simulation of faulted bearings in non-stationary conditions. Meccanica 2018, 53(4-5): 1147-1166, https://doi.org/10.1007/s11012-017-0767-1.
10. Decker J, Lewicki D. Spiral bevel pinion crack detection in a helicopter gearbox. NASA/TM-2003-212327 2003, ARL-TR-2958.
11. Decker J. Crack detection for aerospace quality spur gears. NASA/TM-2002-211492 2002, ARL-TR-2682.

12. Eckmann J, Oliffson K, Ruelle D. Recurrence plots of dynamical systems. Europhysics Letters 1987; 4(9): 973-977, https://doi.org/10.1209/0295-5075/4/9/004.
13. Fraser A M, Swinney H L. Independent coordinates for strange attractors from mutual information. Physical Review A, General Physics 1986; 33(2): 1134-1140, https://doi.org/10.1103/PhysRevA.33.1134.
14. Harsha S P. Nonlinear dynamic response of a balanced rotor supported by rolling element bearings due to radial internal clearance. Mechanism and Machine Theory 2006; 41(6): 688-706, https://doi.org/10.1016/j.mechmachtheory.2005.09.003.
15. Hou Z, Hera A, Noori M. Wavelet-Based Techniques for Structural Health Monitoring. Health Assessment of Engineered Structures: Bridges, Buildings and Other Infrastructure 2013, Chapter 7: 179-201, https://doi.org/10.1142/9789814439022_0007.
16. Huaitao S, Bai X, Zhang K, Wu Y, Wang Z. Effect of thermal-related fit clearance between outer ring and pedestal on the vibration of full ceramic ball bearing. Shock and Vibration 2019, 8357807, https://doi.org/10.1155/2019/8357807.
17. Huang H-Z, Yu K, Huang T, Li H, Qian H-M. Reliability estimation for momentum wheel bearings considering frictional heat. Eksploatacja i Niezawodnosc - Maintenance and Reliability 2020; 22(1): 6-14, https://doi.org/10.17531/ein.2020.1.2.
18. Kennel M B, Brown R, Abarbanel H D I. Determining embedding dimension for phase-space reconstruction using a geometrical construction. Physical Review A 1992; 45(3403), https://doi.org/10.1103/PhysRevA.45.3403.
19. Klimaszewska K, Żebrowski J J. Detection of the type of intermittency using characteristic patterns in recurrence plots. Physical Review E 2009, 80, 026214, https://doi.org/10.1103/PhysRevE.80.026214.
20. Kwuimy C, Samadani M, Kappaganthu K, Nataraj C. Sequential recurrence analysis of experimental time series of a rotor response with bearing outer race faults. Vibration Engineering and Technology of Machinery 2015, 683-696, https://doi.org/10.1007/978-3-319-09918-7_61.
21. Kwuimy C, Samadani M, Nataraj C. Bifurcation analysis of a nonlinear pendulum using recurrence and statistical methods: applications to fault diagnostics. Nonlinear Dynamics 2014, 76: 1963-1975, https://doi.org/10.1007/s11071-014-1261-0.
22. Kwuimy C, Samadani M, Pankar P, Nataraj C. Recurrence analysis of experimental time series of a rotor response with bearing outer race faults. ASME 2015 International Design Engineering Technical Conferences and Computers and Information in Engineering Conference, 2-5 August 2015, Boston, USA, https://doi.org/10.1115/DETC2015-48106.
23. Litak G, Gajewski J, Syta A, Jonak J. Quantitative estimation of the tool wear effects in a ripping head by recurrence plots. Journal of Theoretical and Applied Mechanics 2008; 46(3): 521-530.
24. Litak G, Sawicki J T, Kasperek R. Cracked rotor detection by recurrence plots. Nondestructive Testing and Evaluation 2009; 24(4): 347-351, https://doi.org/10.1080/10589750802570836.
25. Litak G, Syta A, Gajewski J, Jonak J. Detecting and identifying non-stationary courses in the ripping head power consumption by recurrence plots. Meccanica 2010; 45(4): 603-608, https://doi.org/10.1007/s11012-009-9265-4.
26. Litak G, Syta A, Rusinek R. Dynamical changes during composite milling: recurrence and multiscale entropy analysis. The International Journal of Advanced Manufacturing Technology 2011; 56(5): 445-453, https://doi.org/10.1007/s00170-011-3195-8.
27. Liu Y, Zhang Y, Wu Z. Stochastic dynamic analysis of the rotor-bearing system considering the randomness of the radial clearance. Journal of the Brazilian Society of Mechanical Sciences and Engineering 2019; 41: 529, https://doi.org/10.1007/s40430-019-2038-7.
28. Loutridis S J. Gear failure prediction using multiscale local statistics. Engineering Structures 2008; 30(5): 1214-1223, https://doi.org/10.1016/j.engstruct.2007.07.022.
29. Marwan N, Romano M C, Thiel M, Kurths J. Recurrence plots for the analysis of complex systems. Physics Reports 2007; 438(5-6): 237-329, https://doi.org/10.1016/j.physrep.2006.11.001.
30. Meier N, Georgiadis A. Automatic assembling of bearings including clearance measurement. Procedia CIRP 2016; 41: 242-246, https://doi.org/10.1016/j.procir.2015.12.110.
31. Meier N, Papadoudis J, Georgiadis A. Intelligent software system for replacing a force sensor in the case of clearance measurement. Procedia CIRP 2019; 79: 517-522, https://doi.org/10.1016/j.procir.2019.02.103.
32. Miskovic Z, Mitrovic R, Stamenic Z. Analysis of grease contamination influence on the internal radial clearance of ball bearings by thermographic inspection. Thermal Science 2016; 20(1): 255-265, https://doi.org/10.2298/TSCI150319083M.
33. Mitrovic R M, Atanasovska I D, Soldat N D, Momcilovic D B. Effects of operation temperature on thermal expansion and main parameters of radial ball bearings. Thermal Science 2015; 19(5): 1835-1844, https://doi.org/10.2298/TSCI141223091M.
34. Saribulut L, Teke A, Tumay M. Fundamentals and literature review of Fourier transform in power quality issues. Journal of Electrical and Electronics 2013; 5(1): 9-22, https://doi.org/10.5897/JEEER2013.0436.
35. Sawalhi N, Randall R B, Endo H. The enhancement of fault detection and diagnosis in rolling element using minimum entropy deconvolution combined with spectral kurtosis. Mechanical Systems and Signal Processing 2007; 21(6): 2616-2633, https://doi.org/10.1016/j.ymssp.2006.12.002.
36. Sen A K, Litak G, Edwards K D, Finney C E A, Daw C S, Wagner R M. Characteristics of cyclic heat release variability in the transition from spark ignition to HCCI in a gasoline engine. Applied Energy 2011; 88(5): 1649-1655, https://doi.org/10.1016/j.apenergy.2010.11.040.
37. Sharma A, Upadhyay N, Kankar P K, Amarnath M. Nonlinear dynamic investigations on rolling element bearings: A review. Advances in Mechanical Engineering 2018; 10(3): 168781401876414, https://doi.org/10.1177/1687814018764148.
38. Sharma V, Parey A. A review of gear fault diagnosis using various condition indicators. Procedia Engineering 2016; 144: 253-263, https://doi.org/10.1016/j.proeng.2016.05.131.
39. Syta A, Jonak J, Jedliński Ł, Litak G. Failure diagnosis of a gear box by recurrences. Journal of Vibration and Acoustics 2012; 134(4), https://doi.org/10.1115/1.4005846.
40. Takens F. Detecting strange attractors in turbulence. Lecture Notes in Mathematics 1981; 898: 366-381, https://doi.org/10.1007/BFb0091924.
41. Tiwari M, Gupta K, Prakash O. Effect of radial internal clearance of a ball bearing on the dynamics of a balanced horizontal rotor. Journal of Sound and Vibrations 2000; 238(5): 723-756, https://doi.org/10.1006/jsvi.1999.3109.
42. Tomovic R. A simplified mathematical model for the analysis of varying compliance vibrations of a rolling bearing. Applied Sciences 2020; 10(2): 670, https://doi.org/10.3390/app10020670.
43. Torrence C, Compo G P. A practical guide to Wavelet Analysis. Bulletin of the American Meteorological Society 1998, 79(1): 61-7, https://doi.org/10.1175/1520-0477(1998)079<0061:APGTWA>2.0.CO;2.

44. Wang J, Xu M, Zhang C, Huang B, Gu F. Online bearing clearance monitoring based on an accurate vibration analysis. Energies 2020; 13(2): 389, https://doi.org/10.3390/en13020389.
45. Wang W. Early detection of gear tooth cracking using the resonance demodulation technique. Mechanical Systems and Signal Processing 2001; 15(5): 887-903, https://doi.org/10.1006/mssp.2001.1416.
46. Webber C L, Zbilut J P. Dynamical assessment of physiological systems and states using recurrence plot strategies. Journal of Applied Physiology 1994; 76(2): 965-973, https://doi.org/10.1152/jappl.1994.76.2.965.
47. Webber C, Marwan N. Mathematical and computational foundations of recurrence quantifications. Understanding Complex Systems 2015, Chapter 1: 3-43, https://doi.org/10.1007/978-3-319-07155-8_1.
48. Xu M, Feng G, He Q, Gu F, Ball A. Vibration characteristics of rolling element bearings with different radial clearances for condition monitoring of wind turbine. Applied Sciences 2020; 10(14): 4731, https://doi.org/10.3390/app10144731.
49. Yakout M, Nassef M, Backar S. Effect of clearances in rolling element bearings on their dynamic performance, quality and operating life. Journal of Mechanical Science and Technology 2019; 33: 2037-2042, https://doi.org/10.1007/s12206-019-0406-y.
50. Zbilut J P, Webber C L. Embeddings and delays as derived from quantification of recurrence plots. Physics Letters A 1992; 171(3-4): 199-203, https://doi.org/10.1016/0375-9601(92)90426-M.
51. Zhang X, Kang J, Zhao J, Cao D. Features for fault diagnosis and prognosis of gearbox. Chemical Engineering Transactions 2013; 33: 1027-1032, https://doi.org/10.3303/CET1333172.
52. Zhuo Y, Zhou X, Yang C. Dynamic analysis of double-row self-aligning ball bearings due to applied loads, internal clearance, surface waviness and number of balls. Journal of Sound and Vibration 2014; 333(23): 6170-6189, https://doi.org/10.1016/j.jsv.2014.04.054.